JCI insight

Intravital imaging reveals glomerular capillary distension and endothelial and immune cell activation early in Alport syndrome

Georgina Gyarmati, … , Laura Perin, János Peti-Peterdi

JCI Insight. 2021. https://doi.org/10.1172/jci.insight.152676.

Research In-Press Preview Nephrology

Graphical abstract

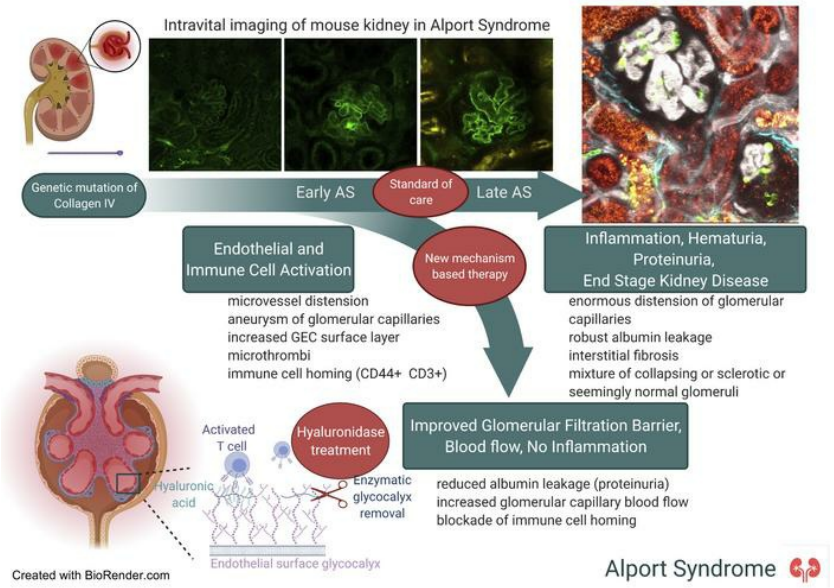

Find the latest version:

https://jci.me/152676/pdf

Intravital imaging reveals glomerular capillary distension and endothelial and immune cell activation early in Alport syndrome

Georgina Gyarmati[1], Urvi Nikhil Shroff[1], Audrey Izuhara[1], Xiaogang Hou[2], Stefano Da Sacco[2], Sargis Sedrakyan[2] Kevin V. Lemley[3], Kerstin Amann[4], Laura Perin,[2*] and János Peti-Peterdi[1*]

[1]Departments of Physiology and Neuroscience, and Medicine, Zilkha Neurogenetic Institute, University of Southern California, Los Angeles, CA, USA

[2]GOFARR Laboratory for Organ Regenerative Research and Cell Therapeutics in Urology, Children's Hospital Los Angeles, Division of Urology, Saban Research Institute, MS #114, University of Southern California, Los Angeles, CA, USA.

[3]Division of Nephrology, Children's Hospital Los Angeles, Los Angeles, CA and Department of Pediatrics, Keck School of Medicine, University of Southern California, Los Angeles, CA, USA

[4]Dept. of Nephropathology, Institute of Pathology, Friedrich Alexander University, Erlangen, Germany

[*]JPP and LP contributed equally to this work.

Co-corresponding authors: * J. Peti-Peterdi, MD, PhD, University of Southern California, 1501 San Pablo Street, ZNI335, Los Angeles, CA 90033; Phone: 323-442-4337, email: petipete@usc.edu

* Laura Perin, PhD, Children's Hospital Los Angeles, Division of Urology, Saban Research Institute, MS #35, University of Southern California, Los Angeles, CA 90027; Phone: 323-361-2247, email: lperin@chla.usc.edu

The authors have declared that no conflict of interest exists.

ABSTRACT

Alport syndrome (AS) is a genetic disorder caused by mutations in type IV collagen that leads to defective glomerular basement membrane, glomerular filtration barrier (GFB) damage, and progressive chronic kidney disease. While the genetic basis of AS is well known, the molecular and cellular mechanistic details of disease pathogenesis have been elusive, hindering the development of mechanism-based therapies. Here we performed intravital multiphoton imaging of the local kidney tissue microenvironment in a X-linked AS mouse model to directly visualize the major drivers of AS pathology. Severely distended glomerular capillaries and aneurysms were found accompanied by numerous microthrombi, increased glomerular endothelial surface layer (glycocalyx) and immune cell homing, GFB albumin leakage, glomerulosclerosis and interstitial fibrosis by 5 months of age with an intermediate phenotype at 2 months. Renal histology in mouse or patient tissues largely failed to detect capillary aberrations. Treatment of AS mice with hyaluronidase or the ACE inhibitor enalapril reduced the excess glomerular endothelial glycocalyx and blocked immune cell homing, and GFB albumin leakage. This study identified central roles of glomerular mechanical forces and endothelial and immune cell activation early in AS, which could be therapeutically targeted to reduce mechanical strain and local tissue inflammation and improve kidney function.

INTRODUCTION

Alport syndrome (AS) is a hereditary form of chronic kidney disease (CKD) caused by mutations in one of the alpha chains of the collagen type IV trimer (*COL4A3/A4/A5*), which is a major constituent of the glomerular basement membrane (GBM) in the glomerular filtration barrier (GFB) (1). The defective GBM causes dysfunction and leakiness of the GFB, development of proteinuria, hematuria, and focal segmental glomerulosclerosis. Regardless of the type of genetic mutation (X-linked, autosomal recessive or dominant AS) and despite diagnosis at an early age, many patients with AS develop progressive CKD and ultimately end-stage kidney disease (1). Although the various genetic mutations leading to AS are well known, mechanistic details of the disease pathogenesis have been elusive, hindering the development of mechanism-based therapies. While the GBM is abnormal already at the time of birth, glomerular function is initially normal, with a delayed onset of dysfunction and progressive disease (2). This observation has important implications about the mechanism of disease initiation. Since only podocytes produce COL4A3/A4/A5, podocyte dysfunction is considered as the major culprit in the pathogenesis of CKD in AS (2). However, AS may not be only a podocyte-driven disease, since our recent work established the role of glomerular endothelial cells (GEC) in early AS (3), and GEC damage is known to precede proteinuria in multiple renal pathologies including AS (4, 5). A mechanistic understanding of AS development is important for the development of specific targeted therapeutic approaches to delay or prevent GFB injury and CKD. Similarly to other types of kidney diseases, the non-specific use of angiotensin converting enzyme (ACE) inhibitors (ACEi) has been the gold-standard treatment to delay the progression of AS (6).

Structural and functional alterations in the local tissue microenvironment are major determinants of disease development and progression. Therefore, the ability to look inside intact

living tissues may provide important mechanistic insights. Intravital imaging with multiphoton microscopy (MPM) is a state-of-the-art technique to visualize dynamic processes in vivo with subcellular resolution, and it has been used in many organs including the kidney to investigate disease pathogenesis (7-9). Most recently, we have used intravital MPM to study interactions between circulating activated T cells and GECs in the local kidney tissue microenvironment in lupus nephritis (10).

In the present work we applied similar in vivo imaging approaches to quantitatively visualize the altered structure and function of the glomerular capillaries, and specifically local GECs and immune cells, during the course of AS development. This focus is consistent with our recently published data that identified the roles of specific immune mechanisms (3) and GEC damage preceding proteinuria development in AS (4). In addition, we tested the therapeutic efficacy of enzymatic glycocalyx removal in AS, since the endothelial surface layer (glycocalyx) is the first point of contact between circulating immune cells and the local tissue environment during inflammation and this treatment approach was found to be protective in experimental lupus nephritis (10).

RESULTS

A new view of AS pathology using intravital MPM imaging

Intravital MPM imaging of the intact kidney tissue microenvironment from early-stage (2 months old) and late-stage (5 months old) AS and healthy age-matched mice was performed to gain new in vivo visual clues regarding alterations in kidney structure and function, and the potential major molecular and cellular mechanistic drivers at play during AS pathogenesis. An overview of the entire kidney cortex area using intravenously injected, fluorescently labeled

albumin to visualize the intravascular space and second harmonic generation (SHG) to visualize fibrillar collagen clearly showed a number of pathological changes in AS compared to control healthy mice. These included enlarged aberrant glomerular capillaries and albumin leakage from glomeruli into the tubular fluid already in early AS (Figs.1A-B). In addition, as a clear sign of disease progression, more severe pathologies were present in late AS, including enormous and irregular distension of glomerular capillaries, robust albumin leakage through the GFB, the presence of tubular protein casts, focal interstitial fibrosis, and a heterogenous mixture of collapsing, sclerotic and seemingly normal glomeruli (Fig.1C).

A closer look at the glomerular microcirculation in AS revealed that the distension of microvessels (capillary diameter >20 μm vs. ~7 μm in control) was especially pronounced at the afferent end of glomerular capillaries and included the terminal portion of the afferent arteriole (Figs. 1D-E). In addition, localized bulging (aneurysm) of glomerular capillaries, microthrombi and albumin-excluding dark (unlabeled) single cells sticking to the capillary wall and blocking capillary blood flow were commonly observed (Figs. 1E-F). Quantitative analysis of glomerular microcirculatory parameters confirmed the significant, progressive increases in glomerular (Fig. 1G), afferent arteriole (AA, Fig. 1H) and glomerular capillary diameters (Fig. 1J), and in glomerular albumin leakage (Fig. 1K) in early and late AS compared to control, while the efferent arteriole (EA) diameter was reduced (Fig. 1I). The progressive deterioration of these microvascular features correlated with not only GFB functional decline (Fig. 1K) but also with reduced podocyte number as quantified based on $p57^{+}$ glomerular cell number and with glomerular endothelial injury as indicated by the increased density of plasmalemma vesicle-associated protein (PLVAP) which has been used as a marker of glomerular endothelial cell (GEC) injury and remodeling (11, 12) (Figs. 1L-P). Increased glomerular tuft PLVAP expression (typical of early AS at 2 month)

preceded the reduction in podocyte number in AS mice (typical of late AS at 5 month) (Fig. 1O-P).

Increased glomerular endothelial surface layer thickness and immune cell homing

To identify and analyze GECs and the albumin-excluding cells observed in the glomerular capillary plasma in more detail, the endothelial surface layer (glycocalyx) and endogenous immune cells were identified using intravenous injection of FITC-labeled wheat germ agglutinin (FITC-WGA) and Alexa Fluor 488-conjugated anti-CD44 antibodies, respectively. Intravital MPM imaging revealed significantly more intense FITC-WGA labeling and thickening of the GEC luminal glycocalyx in AS compared to control (Fig. 2A-D). This alteration of GECs was observed first in a heterogenous, segmental-like pattern in early-stage AS (Fig. 2B), but in a more substantial and homogenous fashion throughout the entire glomerulus in late AS (Fig. 2C).

In addition, fluorescent labeling of endogenous, circulating immune cells found none or only a few $CD44^+$ cells in control glomeruli (Fig. 2E), but a significantly increased number in AS glomeruli (Fig. 2F-H). The homing of $CD44^+$ cells in the AS kidneys was specific to the glomerular microcirculation, while only a few of these cells were found in peritubular capillaries (Fig. 2G). Co-labeling with Alexa Fluor 594-conjugated anti-CD3 antibodies showed an almost complete overlap of the $CD44^+$ and $CD3^+$ cell populations, suggesting that the majority of these immune cells were activated T cells. As with the above microcirculatory parameters, there was a progressive increase in both GEC glycocalyx thickness and $CD44^+$ immune cell glomerular homing in early and late AS (Fig. 2H).

Effects of hyaluronidase (H) and ACEi treatment

To functionally test the pathogenic role of the excess GEC glycocalyx in AS and the effects of its therapeutic targeting, we first performed acute intravenous injections of the glycocalyx-degrading enzyme, hyaluronidase (H), during continuous time-lapse MPM imaging of glomeruli in control and late AS mice. Within 1 hour of injection, acute H treatment (50U) in AS mice significantly reduced the excess GEC glycocalyx thickness to approximately control levels (Fig. 3B, D, E). Simultaneously, H treatment substantially decreased the glomerular homing of $CD44^+$ cells and the immune cells returned to the circulation (Fig. 3A-F, Supplementary Video 1). H treatment in control mice had no significant effects on these parameters (Fig. 3A, C). Importantly, within this short time window (within 1 hour) the removal of excess GEC glycocalyx and $CD44^+$ cell homing by H injection normalized glomerular capillary blood flow (Fig. 3G) and substantially improved GFB barrier function as measured by the reduced glomerular albumin leakage (Fig. 3H).

We next performed chronic administration of either H, enalapril, or control vehicle for one week in late AS mice. H and ACEi treatment equally reduced GEC glycocalyx thickness (Fig. 3I-L) and the number of immune cells/glomerulus (Fig. I-K, M), improved glomerular blood flow (Fig. 3N), and reduced albuminuria (Fig. 3O) compared to control treatment with vehicle (PBS).

Renal histology features of mouse and human AS

Finally, to confirm whether the observed glomerular structural alterations can also be found in mouse or human renal histological sections, we performed histological staining of mouse kidney tissue or renal biopsy specimens from patients with AS (Fig. 4A-B). Glomerular capillary distension was not observed in histological paraffin sections of the same mice that showed the phenotype of capillary aberrations in vivo with MPM (Fig. 4A). A preliminary qualitative analysis

of human AS kidney sections (i. e. from routine diagnostic biopsies) detected the presence of $CD3^+$ and $CD44^+$ immune cells in glomeruli, however distended capillaries were rarely seen (Fig. 4B). Only 5 patient samples showed some minor capillary irregularities out of 34 AS patients examined.

DISCUSSION

The present study applied an unbiased intravital imaging approach using MPM of the local kidney tissue microenvironment to search for direct visual clues concerning the major drivers of AS pathology. The key findings were the clear signs of progressive glomerular endothelial and immune cell activation already in an early phase of disease pathogenesis, and included severely distended glomerular capillaries, aneurysms and microthrombi, increased glomerular endothelial surface layer (glycocalyx) thickness and immune cell homing, and albumin leakage through the damaged GFB. Complementary histological analysis identified and confirmed the increased expression of the GEC injury marker PLVAP (11) in early and late AS and the reduced podocyte number in late AS, consistent with endothelial injury preceding podocyte damage. Interestingly, glomerular capillary distension was not observed in histological paraffin sections of the same mice that showed the phenotype of capillary aberrations in vivo with MPM. While the presence of immune cells in glomeruli was detected in fixed human AS kidney sections suggesting the translatability of at least some of our findings to human disease, distended capillaries were rarely seen in classic histological analysis. Since the newly acquired visual clues pointed to endothelial activation and excess glycocalyx as the main early culprits, a new mechanism-based therapeutic approach was devised and used both as acute and chronic treatment with the glycocalyx degrading enzyme, hyaluronidase, in our animal model for initial proof-of-concept. This treatment had no obvious adverse effects but led to improvements in the structure and function of the GFB and

glomerular capillary blood flow, reduced albuminuria and tissue inflammation. Treatment for one week with hyaluronidase or the gold-standard ACEi therapy reduced to a similar extent GEC glycocalyx thickness and immune cell homing, improved glomerular blood flow and proteinuria, further suggesting the importance of these endothelial alterations in the pathogenesis of CKD in AS. Altogether, this study helps to improve our mechanistic understanding of AS pathogenesis and opens the way for the development of new, mechanism-based therapeutic approaches for AS.

The deposition of aberrant collagen by podocytes that leads to defective GBM, podocyte loss and GFB dysfunction is the currently accepted mechanistic paradigm of AS pathogenesis and disease progression (2). As reported recently, podocyte damage and loss during disease progression is evident and is accompanied by increased proteinuria in both human patients and in the same AS mouse model that was used in the present study. These mice succumb to kidney failure and die at around 6 months of age (3, 4, 12). However, our findings suggest that AS may not be simply a podocyte-driven disease. Our recent work established the role of glomerular endothelial cells (GEC) in early AS (3), and GEC damage is known to precede podocyte loss and proteinuria development in multiple renal pathologies including AS (4, 5). Located on the other side of the defective GBM, GEC injury could be secondary to altered podocyte crosstalk e.g. via altered vascular endothelial growth factor (VEGF) signaling (4). However, GECs may well also be affected by the AS microenvironment independently of podocyte effects.

Conventional histology using paraffin sections has not been able to show distended glomerular capillaries in AS mice or patients, likely due to technical constraints (e. g., normal or elevated capillary pressure was lost during fixation). In contrast, intravital MPM imaging in the present work found robust evidence of distension and aneurysms of glomerular microvessels, primarily the afferent arteriole (AA) and the afferent end of capillaries where the intravascular

pressure is known to be the highest (~60 mmHg) in the glomerular microcirculation (Fig. 1E-F). This finding emphasizes the great advantage and need of using intravital MPM for studying AS in the intact living kidney. The observed capillary aberrations are consistent with a weakened GBM contributing to podocytes' and mesangial cells' lost capability to counter the expansile forces of high capillary pressures. This will only worsen as glomerular sclerosis and loss raise the target single-nephron GFR and hence transcapillary hydrostatic pressures for the remnant glomeruli, which may be why in vivo AA and capillary widening worsens with disease progression. The presence of elevated biomechanical strain of the three glomerular cell types, podocytes, endothelial and mesangial cells, in AS has been predicted and deduced before (13, 14). Based on the visualization of distended glomerular capillaries and AA in vivo in the present study, we speculate that the findings were driven by increased mechanical load.

The second key finding of the present study was the substantially (~3-fold) increased glomerular endothelial surface layer (glycocalyx) thickness (Fig. 2A-D) that was likely due to the activation of GECs in AS. The heterogeneity of FITC-WGA labeling, i. e. intense labeling of significantly thickened glycocalyx in some but not all glomerular capillary segments in early AS (Fig. 2B) is consistent with our recent finding on the identification of distinct GEC subpopulations. and altered expression of GEC glycocalyx components in this condition (3). However, the increased rather than decreased glycocalyx thickness that accompanied glomerular albumin leakage (Fig. 1B-F, K) was an unexpected finding, since according to the current paradigm, the glomerular endothelial glycocalyx is an important permselectivity factor for the GFB. Accordingly, kidney injury models are usually characterized by glomerular endothelial glycocalyx shedding causing albumin leakage, as was also demonstrated in our previous MPM imaging work (15, 16). One exception was lupus nephritis, which was similarly associated with increased GEC

glycocalyx as reported recently (10). These findings suggest that the alterations in GEC glycocalyx per se are not always directly related to proteinuria development (either increased or decreased glycocalyx can be pathogenic) and underscore the importance of additional pathogenic factors and the need for comprehensive functional analysis (such as of immune cell-mediated local inflammation).

The third new phenotypic feature of AS found in the present imaging study was the preferential glomerular homing of immune cells (Fig. 2E-H) that were identified as activated T cells (Figs. 2-3). This finding is consistent with the well-established role of tissue inflammation in AS pathogenesis, although cytokines released by resident kidney cell types (17), and monocytes and lymphocytes resident in the tubulointerstitium (18, 19) rather than in glomeruli have been thought to be the main mechanisms. The preferential glomerular homing of T cells fits well with the excessive GEC glycocalyx which was our other main finding discussed above. Among the many molecular mechanisms of immune cell homing, the binding of the CD44 receptor (highly expressed in T cells) to its main ligand hyaluronic acid (a major component of GEC glycocalyx) is one such mechanism (20, 21) that is likely at play in the glomerular immune cell homing observed in our AS mouse model. The effect of hyaluronidase (H) treatment removing the excess GEC glycocalyx as well as depleting glomerular immune cells (Fig. 3, and further discussed below) is supportive of this notion. The key role of this same CD44-hyaluronic acid interaction in T cell homing was demonstrated recently in lupus nephritis (10).

Enzymatic removal of the excess GEC glycocalyx by H treatment and its beneficial effect on blocking glomerular immune cell homing was directly confirmed by our MPM imaging approach using either acute or chronic treatment (Fig. 3). In acute H treatment, this functional test provided unequivocal evidence supporting the primary role of GECs in AS pathogenesis, and also

a proof-of-concept for the efficacy of therapeutically targeting the excess GEC glycocalyx in AS (Fig. 3A-H). Glomeruli were evaluated within 1 hour after H administration based on previous reports that H effect on capillary glycocalyx was maximal at this time point (22, 23). Importantly, chronic H treatment for one week had similar effects, it reduced the excess glomerular endothelial surface layer, almost completely blocked immune cell homing, improved glomerular capillary blood flow and significantly reduced but did not completely eliminate albumin leakage through the GFB (Fig. 3I-O). These findings suggest that the protective effects of H are sustained over longer time periods, further confirming our recent findings in lupus nephritis (10). In addition, these results strongly suggest the key and primary importance of GECs rather than podocytes or mesangial cells in early AS pathogenesis, although contributions of these other glomerular cell types and the defective GBM to AS are still acknowledged (2, 6, 13, 17). The residual GFB albumin leakage or albuminuria after H treatment (Fig. 3H, O) is also consistent with the classic role of GBM and podocyte mechanisms in AS. Although it has been established that H injection does not affect glomerular charge selectivity or permeability of macromolecules (24), the improvement in glomerular albumin leakage in response to glycocalyx removal in the present study seems paradoxical considering that GEC glycocalyx degradation has previously been linked to pathology development (15, 16). However, the removal of excess glycocalyx and consequent blockade of CD44-hyaluronic acid interaction, led to the depletion of glomerular immune cells likely decreasing local tissue inflammation, the presumed reason for the protective effects of H treatment. Interestingly, H treatment produced similar effects via these same mechanisms in a model of lupus nephritis, raising the possibility that GEC glycocalyx accumulation and its pathogenic effects are more widespread than previously thought (10). Importantly, these results also provided proof-of-concept for the relevance of a glycocalyx-targeting therapy for AS. This

approach may open the way for the future development of more specific and upstream mechanism-based treatments in contrast to the currently used standard of care non-specific therapy with renin-angiotensin system inhibitors or even some newer therapeutic options (6, 25). The anti-inflammatory effect of blocking immune cell homing with H treatment is consistent with the well-known major role of tissue inflammation in AS (2, 6). Interestingly, chronic treatment with the gold-standard ACEi therapy for one week similarly reduced GEC glycocalyx and immune cell homing, improved glomerular blood flow and proteinuria (Fig. 3I-O). These results shed new light on possible novel modes of action for the protective effects of ACE inhibitor therapy (reduced endothelial stress and glycocalyx output), and further suggest the relevance of glycocalyx-targeting therapies and the importance of the observed endothelial alterations in AS.

In summary, the present study identified new structural and functional disease phenotypes of AS based on a novel intravital MPM imaging approach. Our findings strongly suggest that while all three glomerular cell types are involved, GECs may play the primary role in AS disease initiation and early progression. GEC glycocalyx targeting may be a new mechanism-based therapeutic approach identified in this study for early AS.

METHODS

Mice. Transgenic Alport mice (B6.Cg-Col4a5tm1Yseg/J, stock #006283) on C57BL/6 background as developed earlier (26) were purchased from the Jackson Laboratory. AS mouse colonies were bred and maintained at the Children's Hospital Los Angeles in specific pathogen-free quarters according to a homozygous/hemizygous breeding scheme. Early-stage (2 months old) and late-stage (5 months old) male AS and healthy age-matched mice were used in the present study. Animal studies were performed in accordance with guidelines approved by the Institutional

Animal Care and Use Committee at the Children's Hospital Los Angeles and at the University of Southern California.

Intravital multiphoton microscopy (MPM). Under continuous anesthesia (Isoflurane 1–4% inhalant via nose-cone), the left kidney was exteriorized through a flank incision and the animals were placed on the stage of an inverted microscope with the exposed kidney placed in a coverslip-bottomed chamber bathed in normal saline as described previously (7, 8). Body temperature was maintained with a homeothermic blanket system (Harvard Apparatus, Holliston, MA). Alexa Fluor 680-conjugated bovine serum albumin (Thermo Fisher, Waltham, MA) was administered iv. by retro-orbital injections to label the circulating plasma (30 μL iv. bolus from 10 μg/ml stock solution). The images were acquired using a Leica SP8 DIVE multiphoton confocal fluorescence imaging system with a 40 × Leica water-immersion objective (numerical aperture (NA) 1.1) powered by a Chameleon Discovery laser at 960 nm (Coherent, Santa Clara, CA) and a DMI8 inverted microscope's external Leica 4Tune spectral hybrid detectors (emission at 500–530 nm for FITC and Alexa Fluor 488, and 675–750 nm for Alexa Fluor 680, and 475-485 nm for detecting second harmonic generation) (Leica Microsystems, Heidelberg, Germany). The potential toxicity of laser excitation and fluorescence to the cells was minimized by using a low laser power and high scan speeds to keep total laser exposure as minimal as possible. The usual image acquisition (12-bit, 512 × 512 pixel) consisted of only one z-stack tissue volume (xyz with 1 μm steps within < 2 min) or time-lapse (xyt in every 5 s for up to 15 min) collection per glomerulus, which resulted in no apparent cell injury. Image analysis and fluorescence intensity measurements were assessed by LAS X software (3.6.0.20104), Leica Microsystems).

Glomerular hemodynamics. Alexa Fluor 680-conjugated bovine serum albumin was used to label the circulating plasma and the negative labeled (albumin-excluding) red blood cells (RBCs). Glomerular capillary blood flow was evaluated based on measurement of RBC velocity using line (xt) scans of capillary lumen as described before (8). GFB function was evaluated based on measurement of albumin leakage into the Bowman's space (glomerular sieving coefficient, GSC of albumin) (8, 27). Region of interest (ROI) were drawn in glomerular capillary plasma and the Bowman's space, and image analysis was performed as described previously (16, 28).

Endothelial surface layer (GEC glycocalyx) Imaging. FITC-labeled wheat germ agglutinin (FITC-WGA) lectin (Triticum vulgaris; L4895, Sigma, MO), administered via retro-orbital sinus at 2 μg/g body weight was used to visualize the entire glomerular endothelial glycocalyx. FITC-WGA lectin positive region of the glomerular endothelial capillary surface was visible immediately after injection. FITC-WGA lectin fluorescence intensity and thickness were evaluated before and 10 min after H treatment (50 U). Quantification of glycocalyx thickness was performed on capillary wall line profiles by calculating the width of FITC-WGA signal at half-maximum fluorescence intensity as described before (15, 16).

In vivo labeling and analysis of endogenous $CD3^+CD44^+$ T cell homing. Alexa Fluor 594-labeled anti-CD3 antibody (BioLegend, San Diego, CA) and Alexa Fluor 488-labeled anti-CD44 antibodies (BioLegend) were used to detect activated T cells, and to directly and quantitatively visualize their glomerular intravascular homing in WT and AS mice using time-lapse MPM as described recently (10). These antibodies were administered via retro-orbital sinus each at dose of 30 μl. Positively labeled cells could be seen clearly immediately after antibody injection. The

number of CD3 and CD44 double positive cells in entire glomeruli were counted in 3D volume (xyz) images before and after H treatment. Multiple glomeruli per each mouse were analyzed to avoid sampling errors. In some experiments time-lapse imaging of the same z plane was performed for 5-10 minutes, and single projection images of the entire xyt sequence were generated to illustrate the dynamics and magnitude ($CD3^+CD44^+$ cell density) of immune cell surveillance.

Kidney tissue histology. Immunofluorescence detection of proteins was performed as described previously (29). Briefly, kidneys were perfused and fixed in 4% PFA for 2 hours at room temperature, embedded in paraffin, and sectioned 8 μm thick. For antibody stains, slides were washed in 1XPBS. For antigen retrieval, heat-induced epitope retrieval with Sodium Citrate buffer (pH 6.0) or Tris-EDTA (pH 9.0) was applied. To reduce non-specific binding, sections were blocked with normal serum (1:20). Primary and secondary antibodies were applied sequentially overnight at 4º C and 2 hours at room temperature. Primary antibodies and dilutions were as follows: anti-p57 (1:100, Abcam, MA, USA), PLVAP (1:100, Bio-Rad Laboratories, Hercules, CA), CD31 (1:100, Cell Signaling Technology, Danvers, MA). Alexa Fluor 488, 594, and 647-conjugated secondary antibodies were purchased from Invitrogen. Slides were mounted by using DAPI-containing mounting media (VectaShield, Vector Laboratories Inc., Burlingame, CA). Sections were examined with Leica TCS SP8 (Leica Microsystems, Wetzlar, Germany) confocal/multiphoton laser scanning microscope systems as described previously (29-31). In addition, Periodic acid–Schiff (PAS) stained mouse kidney sections (2 μm thick) were imaged and analyzed using the Leica LAS EZ 3.4 software.

Hyaluronidase (H) and ACEi treatment. In acute studies, control and AS mice were given iv via retro-orbital sinus a 0.02 ml bolus of either vehicle (PBS) or H (50 U, Sigma-Aldrich, H3506). The thickness of GEC glycocalyx (width of FITC-WGA signal), the number of CD3 and CD44 positive cells, glomerular capillary blood flow, and albumin GSC in the same glomerulus were measured before and within 1 hour of H treatment. In chronic studies, H (200 U, as above) was given iv every other day for a total of three times as described recently (10). The ACE inhibitor (ACEi) enalapril was administered at a dose of 10 mg/day/mouse via drinking water (150mg/L) as described before (32). Animals were treated with H, ACEi or vehicle (PBS given iv) for one week followed by intravital MPM imaging and tissue harvest as described above. The albumin/creatinine ratio (ACR) was measured from spot urine samples collected on days 0, 1, 3, and 7 using ELISA (10).

AS patient cohort and renal histology. AS diagnosis was made at the Department of Nephropathology, Friedrich-Alexander University (FAU) Erlangen-Nürnberg based on patient family history, clinical data (hematuria, proteinuria), light microscopy, negative immune histology and more specifically electron microscopy of routine kidney biopsy specimen as described recently (33). For the present study, archived toluidine-blue stained semithin sections of routine renal biopsies of 34 AS patients were examined. Immunofluorescence labeling of CD31, CD3 and CD44 positive cells was performed on residual PFA-fixed archived biopsies as described above for mouse kidney tissue sections.

Statistics. Data are reported as means ± SEM, with *n* referring to the number of animals studied. One-way ANOVA with Sydak (for paired experiments) or Tukey's multiple comparison test was performed using GraphPad Prism 8. $P<0.05$ was considered significant.

Study approval

All animal protocols were approved by the Institutional Animal Care and Use Committee at the Children's Hospital Los Angeles and at the University of Southern California. The studies on residual archived human renal biopsies were conducted according to the principles of the Declaration of Helsinki and approved by the ethics committee of the Friedrich-Alexander University Erlangen-Nürnberg (approval number: 251_18 B).

AUTHOR CONTRIBUTIONS

G.G., U.N.S, A.I., X.H., S.D.S, S.S. and K.A. conducted the experiments; G.G., L.P., K.L. and J.P.P. designed the study and wrote the paper.

ACKNOWLEDGMENTS

This work was supported in part by NIH grants R01 DK064324 and DK123564 (to JPP), R01 DK121037 (to LP), and S10 OD021833 (to the USC Multi-Photon Microscopy Core). This work was supported by the GOFARR Fund at Children's Hospital Los Angeles (to LP) and SFB 1350 (TP C02) (to KA).

REFERENCES

1. Kashtan CE, Ding J, Garosi G, Heidet L, Massella L, Nakanishi K, et al. Alport syndrome: a unified classification of genetic disorders of collagen IV α345: a position paper of the Alport Syndrome Classification Working Group. *Kidney Int.* 2018;93(5):1045-51.
2. Cosgrove D, and Liu S. Collagen IV diseases: A focus on the glomerular basement membrane in Alport syndrome. *Matrix Biol.* 2017;57-58:45-54.
3. Soloyan H, Thornton M, Villani V, Khatchadourian P, Cravedi P, Angeletti A, et al. Glomerular endothelial cell heterogeneity in Alport syndrome. *Sci Rep.* 2020;10(1):11414.
4. Sedrakyan S, Villani V, Da Sacco S, Tripuraneni N, Porta S, Achena A, et al. Amniotic fluid stem cell-derived vesicles protect from VEGF-induced endothelial damage. *Sci Rep.* 2017;7(1):16875.
5. Sun YB, Qu X, Zhang X, Caruana G, Bertram JF, and Li J. Glomerular endothelial cell injury and damage precedes that of podocytes in adriamycin-induced nephropathy. *PLoS One.* 2013;8(1):e55027.
6. Omachi K, and Miner JH. Alport Syndrome Therapeutics: Ready for Prime-Time Players. *Trends Pharmacol Sci.* 2019;40(11):803-6.
7. Hackl MJ, Burford JL, Villanueva K, Lam L, Susztak K, Schermer B, et al. Tracking the fate of glomerular epithelial cells in vivo using serial multiphoton imaging in new mouse models with fluorescent lineage tags. *Nat Med.* 2013;19(12):1661-6.
8. Kang JJ, Toma I, Sipos A, McCulloch F, and Peti-Peterdi J. Quantitative imaging of basic functions in renal (patho)physiology. *Am J Physiol Renal Physiol.* 2006;291(2):F495-502.
9. Peti-Peterdi J, Kidokoro K, and Riquier-Brison A. Novel in vivo techniques to visualize kidney anatomy and function. *Kidney Int.* 2015;88(1):44-51.

10. Kadoya H, Yu N, Schiessl IM, Riquier-Brison A, Gyarmati G, Desposito D, et al. Essential role and therapeutic targeting of the glomerular endothelial glycocalyx in lupus nephritis. *JCI Insight.* 2020;5(19).

11. Ichimura K, Stan RV, Kurihara H, and Sakai T. Glomerular endothelial cells form diaphragms during development and pathologic conditions. *J Am Soc Nephrol.* 2008;19(8):1463-71.

12. Sedrakyan S, Da Sacco S, Milanesi A, Shiri L, Petrosyan A, Varimezova R, et al. Injection of amniotic fluid stem cells delays progression of renal fibrosis. *J Am Soc Nephrol.* 2012;23(4):661-73.

13. Kriz W, Elger M, Mundel P, and Lemley KV. Structure-stabilizing forces in the glomerular tuft. *J Am Soc Nephrol.* 1995;5(10):1731-9.

14. Wyss HM, Henderson JM, Byfield FJ, Bruggeman LA, Ding Y, Huang C, et al. Biophysical properties of normal and diseased renal glomeruli. *Am J Physiol Cell Physiol.* 2011;300(3):C397-405.

15. Butler MJ, Ramnath R, Kadoya H, Desposito D, Riquier-Brison A, Ferguson JK, et al. Aldosterone induces albuminuria via matrix metalloproteinase-dependent damage of the endothelial glycocalyx. *Kidney Int.* 2018.

16. Salmon AH, Ferguson JK, Burford JL, Gevorgyan H, Nakano D, Harper SJ, et al. Loss of the endothelial glycocalyx links albuminuria and vascular dysfunction. *J Am Soc Nephrol.* 2012;23(8):1339-50.

17. Warady BA, Agarwal R, Bangalore S, Chapman A, Levin A, Stenvinkel P, et al. Alport Syndrome Classification and Management. *Kidney Med.* 2020;2(5):639-49.

18. Lebleu VS, Sugimoto H, Miller CA, Gattone VH, 2nd, and Kalluri R. Lymphocytes are dispensable for glomerulonephritis but required for renal interstitial fibrosis in matrix defect-induced Alport renal disease. *Lab Invest.* 2008;88(3):284-92.

19. Rodgers KD, Rao V, Meehan DT, Fager N, Gotwals P, Ryan ST, et al. Monocytes may promote myofibroblast accumulation and apoptosis in Alport renal fibrosis. *Kidney Int.* 2003;63(4):1338-55.

20. McDonald B, and Kubes P. Interactions between CD44 and Hyaluronan in Leukocyte Trafficking. *Front Immunol.* 2015;6:68.

21. McDonald B, McAvoy EF, Lam F, Gill V, de la Motte C, Savani RC, et al. Interaction of CD44 and hyaluronan is the dominant mechanism for neutrophil sequestration in inflamed liver sinusoids. *J Exp Med.* 2008;205(4):915-27.

22. Henry CB, and Duling BR. Permeation of the luminal capillary glycocalyx is determined by hyaluronan. *Am J Physiol.* 1999;277(2 Pt 2):H508-14.

23. VanTeeffelen JW, Brands J, Jansen C, Spaan JA, and Vink H. Heparin impairs glycocalyx barrier properties and attenuates shear dependent vasodilation in mice. *Hypertension.* 2007;50(1):261-7.

24. Sverrisson K, Axelsson J, Rippe A, Asgeirsson D, and Rippe B. Dynamic, size-selective effects of protamine sulfate and hyaluronidase on the rat glomerular filtration barrier in vivo. *Am J Physiol Renal Physiol.* 2014;307(10):F1136-43.

25. Torra R, and Furlano M. New therapeutic options for Alport syndrome. *Nephrol Dial Transplant.* 2019;34(8):1272-9.

26. Rheault MN, Kren SM, Thielen BK, Mesa HA, Crosson JT, Thomas W, et al. Mouse model of X-linked Alport syndrome. *J Am Soc Nephrol.* 2004;15(6):1466-74.

27. Peti-Peterdi J, and Sipos A. A high-powered view of the filtration barrier. *J Am Soc Nephrol.* 2010;21(11):1835-41.

28. Nakano D, Kobori H, Burford JL, Gevorgyan H, Seidel S, Hitomi H, et al. Multiphoton imaging of the glomerular permeability of angiotensinogen. *J Am Soc Nephrol.* 2012;23(11):1847-56.

29. Riquier-Brison ADM, Sipos A, Prokai A, Vargas SL, Toma L, Meer EJ, et al. The macula densa prorenin receptor is essential in renin release and blood pressure control. *Am J Physiol Renal Physiol.* 2018;315(3):F521-f34.

30. Schiessl IM, Fremter K, Burford JL, Castrop H, and Peti-Peterdi J. Long-Term Cell Fate Tracking of Individual Renal Cells Using Serial Intravital Microscopy. *Methods Mol Biol.* 2019.

31. Shroff UN, Schiessl IM, Gyarmati G, Riquier-Brison A, and Peti-Peterdi J. Novel fluorescence techniques to quantitate renal cell biology. *Methods Cell Biol.* 2019;154:85-107.

32. Gyarmati G, Shroff UN, Riquier-Brison A, Kriz W, Kaissling B, Neal CR, et al. A new view of macula densa cell microanatomy. *Am J Physiol Renal Physiol.* 2021;320(3):F492-f504.

33. Braunisch MC, Büttner-Herold M, Günthner R, Satanovskij R, Riedhammer KM, Herr PM, et al. Heterozygous COL4A3 Variants in Histologically Diagnosed Focal Segmental Glomerulosclerosis. *Front Pediatr.* 2018;6:171.

FIGURE LEGENDS

Figure 1

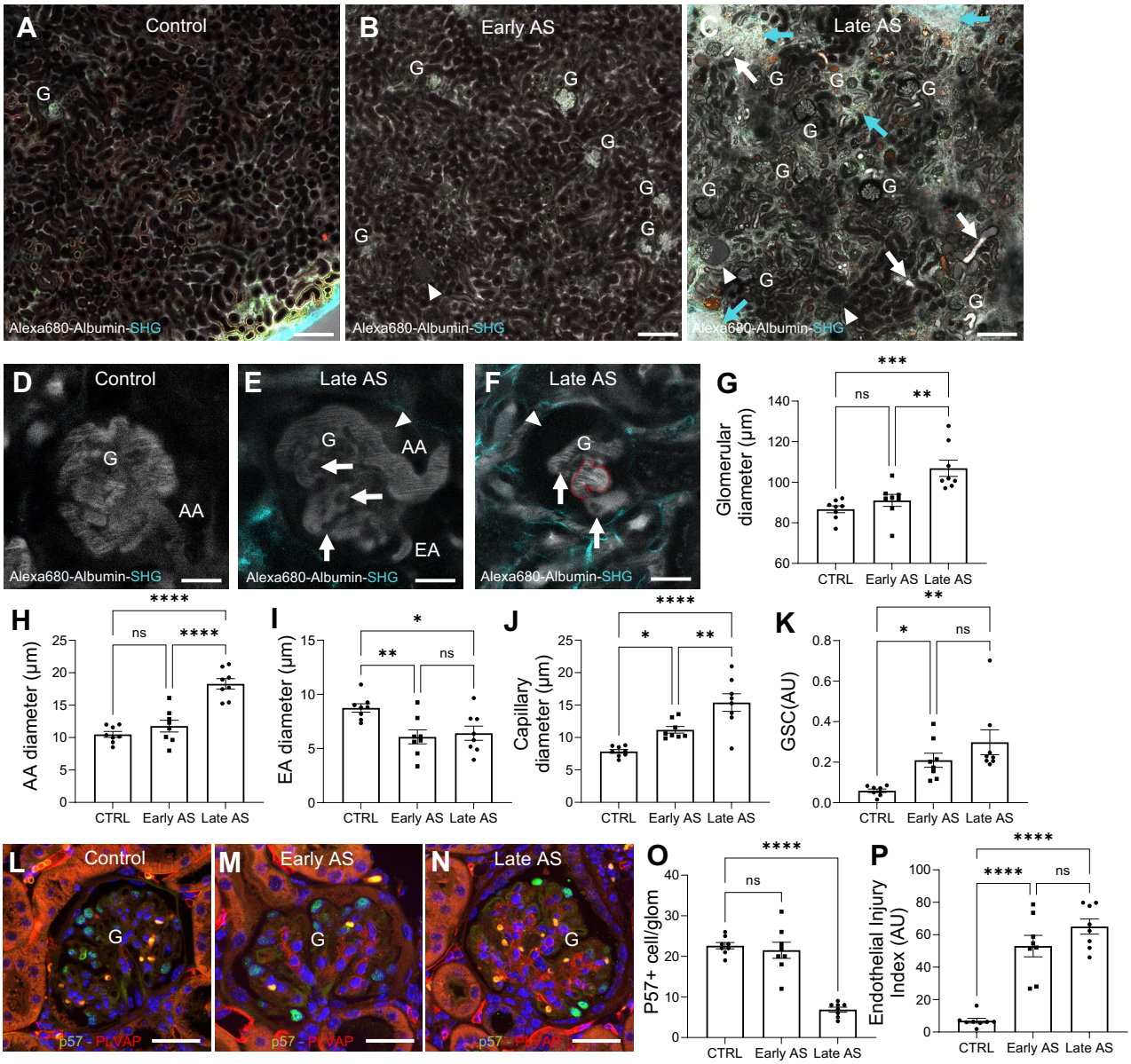

Figure 1. Overview MPM images and microvascular features of AS pathology in the intact living mouse kidney. (A-C): Overview of the renal cortex in 2 months old control (A) and AS (Early AS, B) and 5 months old AS mice (Late AS, C). Plasma was labeled with albumin-Alexa Fluor 680 (grey), and second harmonic generation (SHG, cyan) illuminated fibrotic tissue regions (cyan arrows). G: glomerulus. Bars are 100 µm. Optical sections were acquired approximately 150 µm under the kidney surface. Note the presence of normal glomeruli (no albumin filtration) among albumin-leaking and collapsing glomeruli (arrowheads, grey filtration space in G and tubular lumen) and tubular protein casts (white arrows) in AS mice (B-C), but not in control (A). (D-F) Close-up images of glomeruli in late AS (E-F) compared to control (D) demonstrate severe distension of the afferent arteriole (AA) and glomerular capillaries, the presence of capillary aneurysms (red dotted line illustrates capillary wall), microthrombi and albumin-excluding dark cells (arrows) sticking to capillary walls and blocking red blood cell passage (dark bands in the light grey plasma), robust GFB albumin leakage (arrowheads), and interstitial fibrosis (SHG, cyan). Bars are 20 µm. (G-K) Statistical summary of the changes in largest glomerular (G), afferent arteriole (AA, H), efferent arteriole (EA, I), and glomerular capillary diameters (J), and glomerular albumin leakage (albumin glomerular sieving coefficient (GSC), K) in early and late AS compared to control (CTRL). (L-P) Representative immunofluorescence images (L-N) and quantification (O-P) of the number of podocyte marker $p57^{+}$ cells per glomerular section (green) and the $PLVAP^{+}$ (glomerular endothelial injury marker, red) area of the glomerular tuft in control, early and late AS. Nuclei are stained blue with DAPI. Bars are 20 µm. Values are expressed as means ± SEM, *P< 0.05, **P<0.01, ***P<0.001, ****P< 0.0001 using one-way ANOVA with Tukey's multiple comparison test. Data points represent the average of multiple measurements/mouse for n=8 mice in each group.

Figure 2

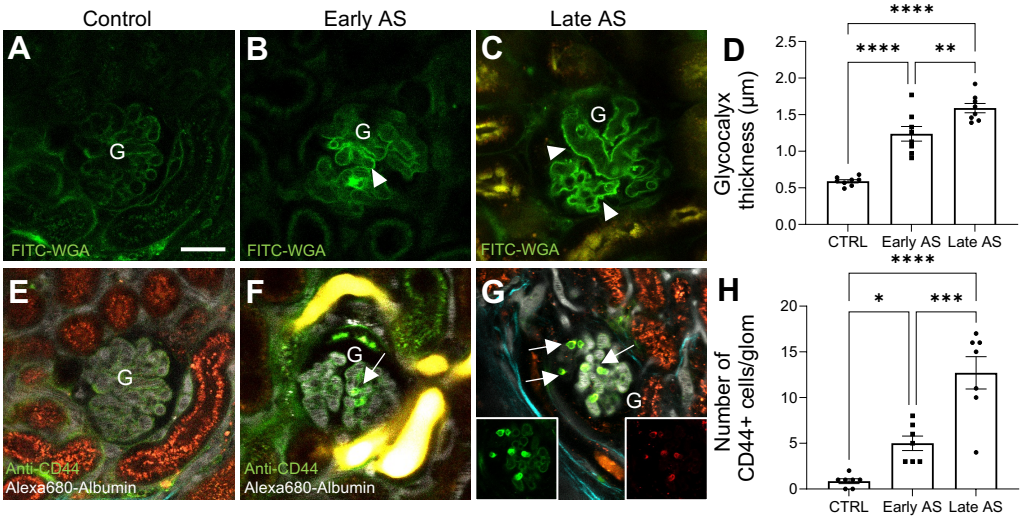

Figure 2. Intravital MPM imaging of glomerular endothelial (A-D) and immune cell features (E-H) in control and AS mice. The endothelial surface layer (glycocalyx) was labeled with FITC-WGA lectin (green, linear pattern along capillary lumen), while circulating immune cells were identified with anti-CD44-Alexa Fluor 488 antibodies (green, round single cell pattern), both injected iv. (**A-D**) Representative images and statistical summary of the significantly increased FITC-WGA intensity and thickness of the GEC glycocalyx (arrowheads) compared to control (**A**) in a segmental pattern in early AS (**B**) and in a global, homogenous pattern in late AS (**C**). (**E-H**) Representative images and statistical summary of the increased number of $CD44^+$ immune cells (arrows) in control and AS mice. Tissue autofluorescence is shown in orange. Note the lack of $CD44^+$ cells in peritubular capillaries. Panel G is an overlay of anti-CD44-Alexa Fluor 488 (green, left inset) and anti-CD3-Alexa Fluor 594 antibody labeling (red, right inset). G: glomerulus. Scale bar is 20 µm. Values are expressed as means ± SEM, ****P< 0.0001 using one-way ANOVA with Tukey's multiple comparison test, data points represent the average of multiple measurements /mouse for n=8 mice in each group.

Figure 3

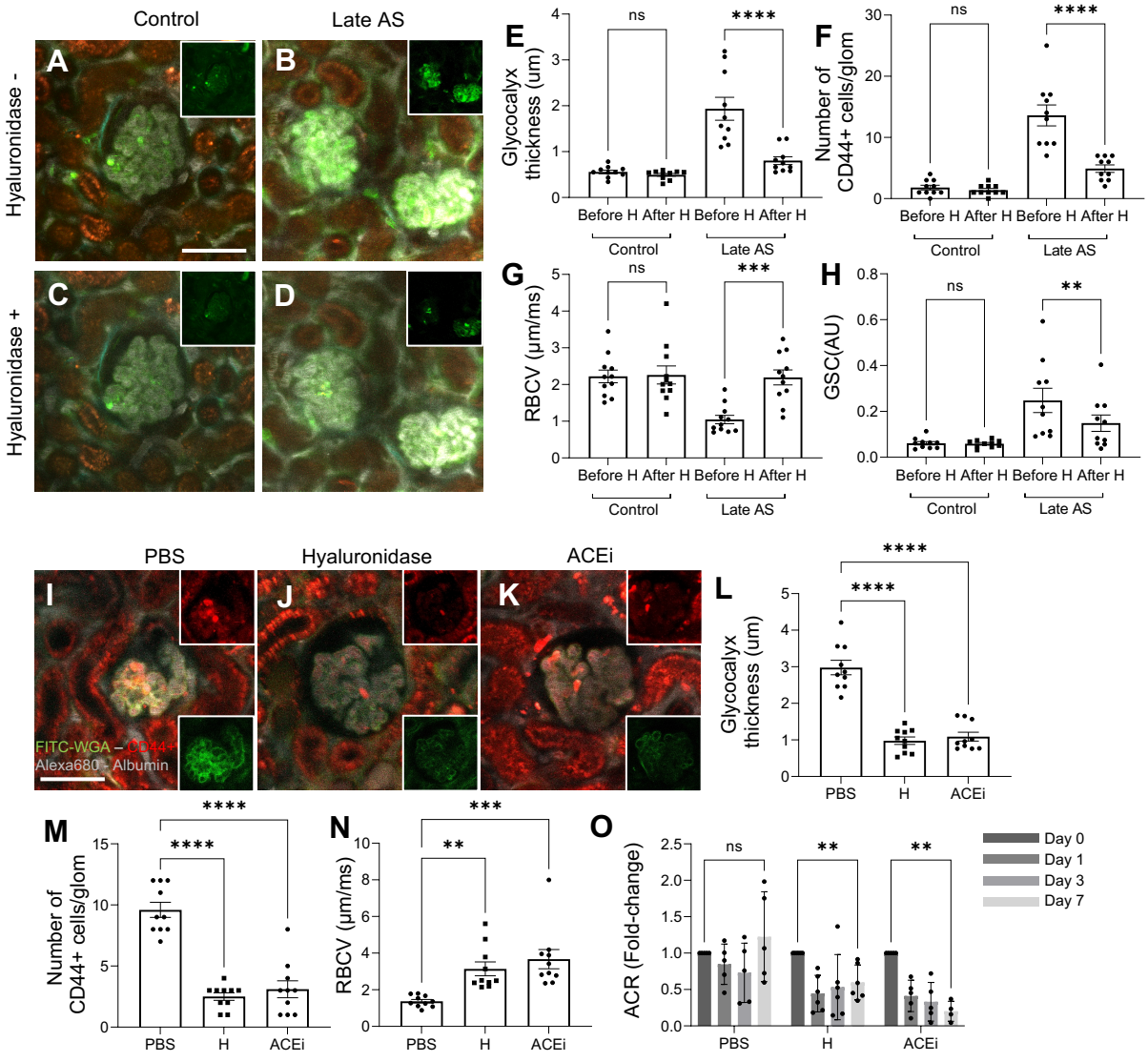

Figure 3. Time-lapse in vivo MPM imaging of the effects of hyaluronidase (H) and ACEi treatment in late AS mice. (A-H) Acute H treatment in control (A, C) and late AS (B, D). Plasma was labeled with albumin-Alexa Fluor 680 (grey), glycocalyx with FITC-WGA lectin (green, linear pattern), immune cells with anti-CD44-Alexa Fluor 488 antibodies (green, round cell pattern). (A-D) Projection images of 5 min time-lapse (overlay of plasma albumin (grey), glycocalyx and immune cell labeling (green), tissue autofluorescence (orange), insets show glycocalyx and CD44$^+$ cell separately) of the glomerular microenvironment before (A-B) and within 1 hour of iv H (50 U) injection (C-D) in control (A,C) and late AS (B,D). Note the high glomerular capillary albumin intensity in late AS and its reductions after H treatment (B, D) indicating improved blood flow (flow of non-fluorescent red blood cells (RBC) rather than only the highly fluorescent plasma, Supplementary Video 1). (E-H) Summary of the effects of H treatment in control and late AS on GEC glycocalyx thickness (E), CD44+ cell number per glomerulus (F), glomerular capillary blood flow (RBC velocity, G), and glomerular albumin leakage (albumin GSC, H). (I-O) Chronic treatment with H, ACEi, or control PBS for one week in late AS. Projection images of 5 min time-lapse as in A-D (insets show glycocalyx (green) and CD44$^+$ cells (red) separately) in control vehicle (PBS)(I), H (J), and ACEi treatment groups (K). (L-O) Summary of the effects of control PBS, H, or ACEi treatment on GEC glycocalyx thickness (L), CD44+ cell number per glomerulus (M), glomerular capillary blood flow (N), and albuminuria (albumin/creatinine ratio (ACR), O). Values are expressed as means ± SEM, ** p<0.01, *** p<0.001, **** p<0.0001, ns: not significant using one-way ANOVA followed by Tukey's or Sidak's multiple comparison test. Bar is 50 µm for all panels. Data points represent the average of multiple measurements/mouse (O) or from 2 glomeruli/mouse (E-N), n=5-6 mice in each group.

Figure 4

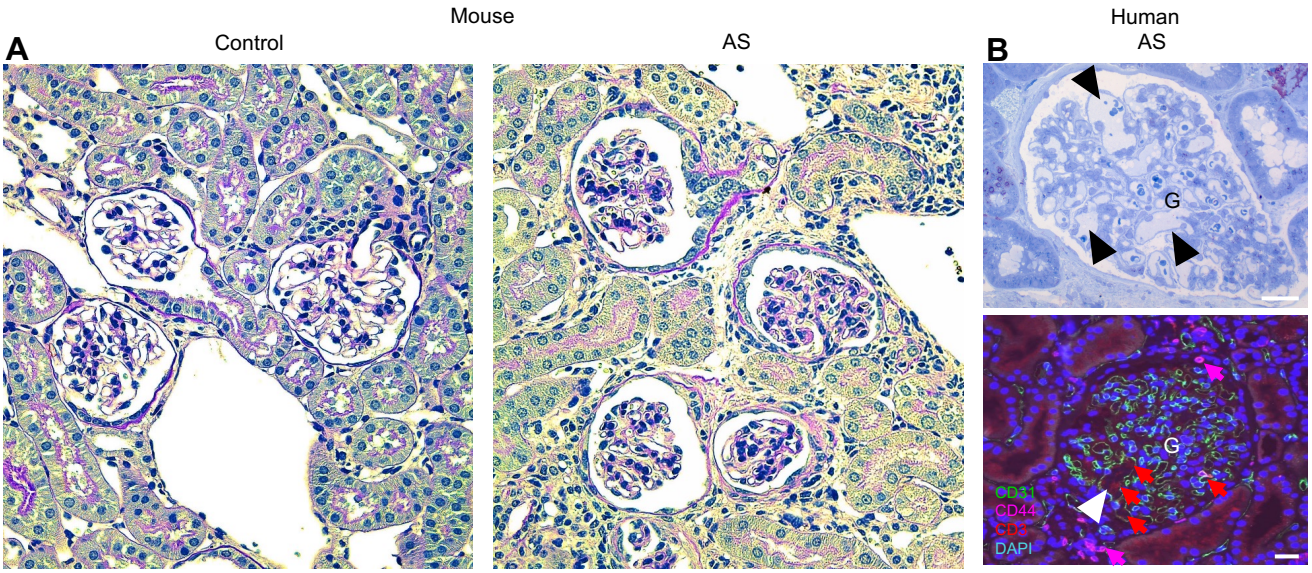

Figure 4. Histological features of mouse (A) and human kidney tissue (B) AS sections. (A) PAS-stained thin sections of the kidney tissue of same mice that were used for intravital imaging. Note the lack of severely distended glomerular capillaries in either control or AS tissues. **(B)** Representative semithin section with toluidine blue staining (top) of 5 out of 34 AS patient samples and paraffin section with immunofluorescence multi-labeling (bottom) for CD31 (green), CD44 (purple) and CD3 (red). Note the presence of distended glomerular capillaries (arrowheads) and $CD44^+$ and $CD3^+$ immune cells in the glomerular capillary lumen (red and purple arrows) in these specific human AS sections. Nuclei are stained blue with DAPI. Bars are 20 μm.

Visual Abstract

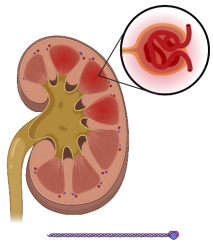

Intravital imaging of mouse kidney in Alport Syndrome

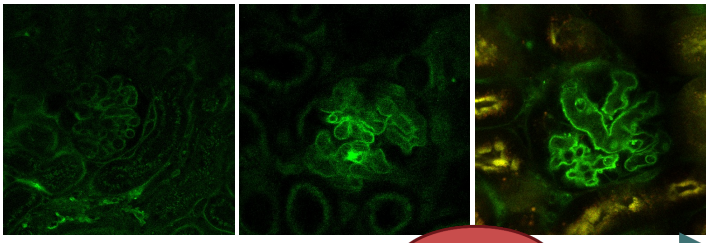

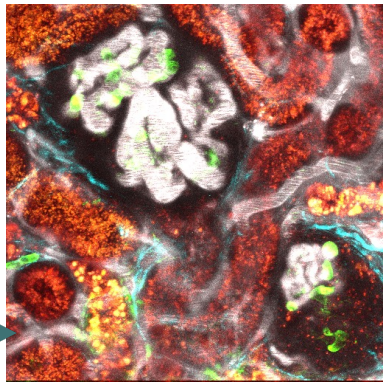

Genetic mutation of Collagen IV

Early AS

Standard of care

Late AS

Endothelial and Immune Cell Activation

microvessel distension
aneurysm of glomerular capillaries
increased GEC surface layer
microthrombi
immune cell homing (CD44+ CD3+)

New mechanism based therapy

Inflammation, Hematuria, Proteinuria, End Stage Kidney Disease

enormous distension of glomerular capillaries
robust albumin leakage
interstitial fibrosis
mixture of collapsing or sclerotic or seemingly normal glomeruli

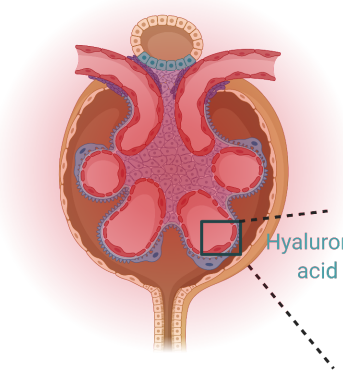

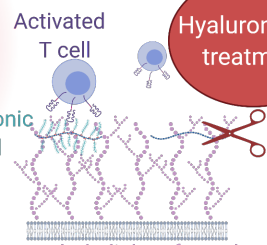

Hyaluronidase treatment

Enzymatic glycocalyx removal

Improved Glomerular Filtration Barrier, Blood flow, No Inflammation

reduced albumin leakage (proteinuria)
increased glomerular capillary blood flow
blockade of immune cell homing

Created with BioRender.com

Alport Syndrome